Prediction of the dynamic behavior of an uncertain friction system coupled to nonlinear energy sinks using a multi-element generalized polynomial chaos approach

Cherif Snoun, Baptiste Bergeot, Sébastien Berger

Prediction of the dynamic behavior of an uncertain friction system coupled to nonlinear energy sinks using a multi-element generalized polynomial chaos approach

Cherif Snoun, Baptiste Bergeot*, Sébastien Berger

INSA CVL, Univ. Orléans, Univ. Tours, LaMé EA 7494, F-41034, 3 Rue de la Chocolaterie, CS 23410, 41034 Blois Cedex, France

Abstract

In this paper, a friction system with uncertain parameters and coupled to two Nonlinear Energy Sinks (NESs) is studied. The dispersion of some physical parameters due to their uncertain nature may generate a dynamic instability which leads to a Limit Cycle Oscillations (LCO) causing a propensity of squeal. The concept of Targeted Energy Transfer (TET) by means of NESs to mitigate this squealing noise is proposed. In this kind of unstable dynamical system coupled to NES, the transition from harmless regimes (i.e. the LCO is mitigated) to harmful regimes (i.e. the LCO is not mitigated) as a function of the uncertain parameters implies a discontinuity in the steady-state amplitude profiles. In this context, a Multi-Element generalized Polynomial Chaos (ME-gPC) based method is proposed to locate this discontinuity (called mitigation limit) and therefore to predict the Propensity of the system to undergo an Harmless Steady-State Regime (PHSSR). The results obtained with this original method lead to a good compromise between computational cost and accuracy in comparison with a reference method.

Keywords: Friction-induced vibration, Nonlinear Energy Sink, Uncertainty, Robust modeling, Multi-Element generalized Polynomial Chaos

1. Introduction

Unwanted vibrations due to Limit Cycle Oscillations (LCO) generated by dynamic instabilities are encountered in a numerous industrial applications. Dry friction systems are good examples of these systems (Chevennement-Roux et al. (2007); Sinou and Jézéquel (2007)). They undergo dynamic instabilities related to the friction. A way to explain these instabilities is the so-called sprag-slip mechanism and more generally the mode-coupling phenomenon. In most self-excited friction system, the instability is due to mode-coupling phenomenon (Fritz et al. (2007); Oden and Martins (1985)) which is under consideration in this paper. Moreover, several papers as D'Souza and Dweib (1990); Eriksson and Jacobson (2001); Hoffmann and Gaul (2003) showed that the well-known two degrees of freedom Hultèn's model (Hultén (1997, 1993)) is an useful way to investigate the mode-coupling instability. After an exponential transient growth of its amplitude, the unstable friction system saturates to the LCO that may affect their efficiency and the user comfort because of the generation of squeal noise (Kinkaid et al. (2003); Wang et al. (2016)). In recent years, particular attention has been paid to understand the mechanisms generating noise and to predict it in probabilistic approach incorporating uncertainty in the model parameters (Tison et al. (2014); Lü and Yu (2014); Renault et al. (2016)). In fact, uncertainty might have a large effect on the performance of the friction system. Developing strategies to control instabilities is therefore crucial. The classical example from mechanical engineering has been the addition of a vibration absorber to the main system.

Over the past decade, vibrations mitigation using Nonlinear Energy Sinks (NESs) has been a major interest in different engineering applications. The NESs are strongly nonlinear vibration absorber whose operation is relies on the concept of Targeted Energy Transfer (TET). TET have been studied a lot, for example in their seminal paper, Vakakis and Gendelman (2001) analyzed TET in terms of resonance capture. Moreover, it has been shown that the NESs are very efficient for vibration mitigation (Vakatis et al. (2008)) and noise reduction (Bellet et al. (2010)). Depending on the type of the nonlinearity, the NESs can be classified as a cubic NESs (the most common NESs), a vibro-impact NESs (Gendelman (2012)), a piece-wise NESs (Lamarque et al. (2011)) or a rotational NESs Sigalov et al. (2012). In this paper, the cubic NESs are considered. Because this type of nonlinearity, NESs can adjust their frequency to that of the primary system subject to unwanted vibrations. The NESs can therefore dissipate energy over a wide range of frequencies. In the review paper, Lee et al. (2008) discus the recent efforts to passively mitigate unwanted vibrations from a primary structure to NESs by utilizing TET.

*Corresponding author

Email address: baptiste.bergeot@insa-cvl.fr (Baptiste Bergeot)

NESs are also used in the context of instability mitigation. They allow to mitigate or even suppress the instability and to enlarge the area of stability of a primary system. The possible mitigation of the LCO of a Van der Pol oscillator using NESs is demonstrated numerically in Lee et al. (2006) and a theoretical method allowing the prediction of the regime has been proposed in Gendelman and Bar (2010). Lee et al. (2007a,b) demonstrated numerically and experimentally that NESs can be effectively used to perform aeroelastic instability suppression. The authors observed the four typical steady-state regimes resulting of the NESs coupling: complete suppression, mitigation through periodic response, mitigation through strongly modulated response and no suppression of the instability. These results have been proved theoretically by an asymptotic analysis by Gendelman et al. (2010). Bergeot et al. (2016, 2017a) observed these regimes to perform the capacity of NESs to control helicopter ground resonance instability. In this paper, following Bergeot and Bellizzi (2018), the four typical regimes are classified into two categories depending on whether the NESs mitigate or not the instability and therefore separating mitigated situations from unmitigated situations. In recent work by the authors (Bergeot et al. (2017b)), the effect of using NESs to control mode coupling instability in a friction system have been studied. To achieve that, the Hultèn's model is coupled to two NESs. Again the regimes described above have been observed and authors proposed analytical approach which allows to explain and predict some them. The difficulties encountered to differentiate, in the parameters space, mitigated situations from unmitigated situations have been solved in Bergeot and Bellizzi (2019). It has been shown that the transition from mitigated regimes to unmitigated regimes with respect to a parameter variation can involve a discontinuity in the steady-state amplitude profiles. This makes the behavior of the system extremely sensitive to design parameters. As, in the friction systems, the parameters as the friction coefficient and the damping coefficient can undergo a large dispersion, the efficiency of the NESs may be more or less high depending on the values of the uncertain parameters. A slight variation of the value of an uncertain parameter may lead a strong change in the dynamical behavior of the primary system coupled with NESs. Thus, the parametric uncertainties may have a strong influence on the propensity to be in a mitigated regime, in others words, the Propensity to undergo a Harmless Steady-State regime (PHSSR). Hence, it becomes necessary to take into account these uncertainties in the study of the dynamical behavior of the system.

Several probabilistic approaches are used for propagating uncertainties in a deterministic model (DM) of a mechanical system and for evaluating the statistical characteristics or/and the distribution law of a quantity of Interest (QoI) which is a response from the DM. A review on the numerical methods for stochastic prediction can be found in Schuëller (2001), or more recently in Nouy (2009). Monte Carlo (MC) method is a well-known technique in this field (Fishman (1996)) and often used as a reference. However, it may require a huge number of DM evaluations (i.e. high computational cost). Methods such as the generalized Polynomial Chaos (gPC) and the Multi-Element generalized Polynomial Chaos (ME-gPC), have been developed as a less costly alternative to the MC approach. These methods expand the quantity of interest of the DM in series of polynomials of uncertain variables. The coefficients of the expansion, i.e. the gPC coefficients, are deterministic. They are the unknowns of the problem and therefore must be evaluated, using either intrusive or non-intrusive methods. In the intrusive method, modifications of DM are requested to determine the gPC coefficients which may be inconvenient in a industrial context. The non-intrusive strategy only requires a number of simulations of DM to obtain the gPC coefficients, this approach is used in this paper. The gPC has been used to perform stochastic analysis of the dynamic behavior of friction systems in Sarrouy et al. (2013). For instance, Nechak et al. (2013) studied the stability of a break system using the indirect Lyapunov approach associated with a non-intrusive gPC. Uncertainties due to friction in gear system have been investigated using the gPC in Guerine et al. (2016). Moreover, the ME-gPC is shown to be very efficient to predict the friction-induced vibrations in a nonlinear uncertain dry friction system Nechak et al. (2011, 2012). More recently in Trinh et al. (2016), the ME-gPC has been used to perform stability analysis of a clutch system, a significant reduction of the computational cost in comparison with the standard gPC has been highlighted.

As described above, TET and NESs have been studied extensively in a deterministic context but there is very little works performing stochastic approach. In Gourdon and Lamarque (2006), by means gPC approach the effects on the NESs behavior during instationary regimes in a two DOF academic system are analyzed by introducing uncertain parameters to verify the robustness of the TET when parameters are not well known. In Sapsis et al. (2011) a TET problem from a linear medium to a nonlinear attachment is studied in the presence of stochasticity. The approach leads to a stochastic differential equation which is numerically solved. The analysis reveals that in presence of uncertain parameters the optimal TET regimes, predicted in a deterministic context, are preserved and even enhanced because of the interaction between nonlinearity and stochasticity. Cataldo et al. (2013) studied the TET robustness considering a one linear DOF coupled to one NESs with three uncertain parameters. Moreover, Boroson et al. (2017) investigated the optimization of multiple NESs configured in parallel taking into account uncertainties in the design optimization of parallel NESs. Therefore no study have been achieved to analyze the dynamical behavior of an unstable friction system with NESs taking account uncertain parameters.

As explained above, a friction system coupled to NESs may be in a regime with harmful Limit cycle Oscillation

or not according to the values of the uncertain parameters. Moreover, the transition from the mitigated regimes to the unmitigated regimes as a function of these uncertain parameters implies a discontinuity in the steady-state amplitude profiles (the amplitude will be the QoI in this paper). The objective of this paper is therefore to develop a method to locate this discontinuity in the dynamical behavior of a friction system coupled to two NESs and then to predict, with a low computational cost, the PHSSR, being given the probability density function of the uncertain parameters. The goal is not to obtain an accurate representation of the QoI but to be able to locate the discontinuity. This allows to determine the PHSSR of the system which corresponds to the region of the uncertain parameters space in which the steady-state regime is harmless . For this purpose, an original method based on the ME-gPC will be established and applied on the Hultèn's model coupled to two NESs.

This paper is organized as follows. The gPC and the ME-gPC formalisms are presented in Sect. 2. In Sect. 3, the proposed method, using ME-gPC, to locate a discontinuity in the quantity of interest profile is described. Sect. 4 describes the system under study which consists in the two DOF Hultén's model coupled to two NESs. The possible steady-state regimes resulting of the NESs attachments are presented in Sect. 5. In Sect. 6, the method presented in Sect. 3 is applied to locate the discontinuity in the steady-state amplitude profiles and then to compute PHSSR of the system under study. Moreover, for validation purposes, the method is compared to a reference method. Finally, conclusions perspectives are given in Sect. 7.

2. Polynomial Chaos theory

2.1. Generalized Polynomial Chaos (gPC)

Let $\beta = (\beta_1, ..., \beta_r)$ the vector of r uncertain physical parameters supposed to be uniformly distributed within a given space $\prod_{i=1}^{r}[a_i, b_i]$. Let $\xi = (\xi_1, ..., \xi_r)$ is the vector of r independent random variables within the space $[-1\ 1]^r$ and linked to $\beta(\beta_1, ..., \beta_r)$ by

$$\beta_j(\xi_j) = \frac{a_j + b_j}{2} + \frac{b_j - a_j}{2}\xi_j, \quad (j = 1, \ldots, r). \tag{1}$$

From the gPC theory (Xiu and Karniadakis (2002); Cameron and Martin (1947); Wiener (1938)), a second order process, so called quantity of Interest (QoI), may be approximated by a truncated orthogonal Legendre polynomial function series as

$$X(\xi) \approx \sum_{j=0}^{N_p} \bar{x}_j \phi_j(\xi), \tag{2}$$

where $\phi_j(\xi)$ are orthogonal polynomials constructed from Legendre polynomials which represent the stochastic part of the process whereas gPC coefficients $\bar{x}_j$ which take into account the deterministic part of the process.

Therefore to obtain the approximated values of the QoI X the coefficients $\bar{x}_j$ of the truncated series Eq. (2) must be computed. From Xiu and Karniadakis (2002), the number of terms $N_p + 1$ is given by the following expression

$$N_p + 1 = \frac{(p + r)!}{p!r!}, \tag{3}$$

where r is the number of uncertain parameters and p is the order of the gPC.

As mentioned previously, the gPC coefficients can be determined either from intrusive methods or from non-intrusive methods. In this paper, non-intrusive methods are preferred because they are more suitable in an industrial context. Indeed, they do not require to modify the DM of the mechanical system as explained in the previous section; the gPC coefficients are built from a quite number of values of the QoI X, obtained from numerical simulations of the DM of the mechanical system. The non-intrusive method used in this paper is the regression method (Berveiller et al. (2006)) which requires a minimum of $Q = N_p$ simulations to built the coefficients. These Q simulations may be performed at points chosen with the Latin Hypercube Samples (LHS) method (McKay et al. (1979)) and will be called Numerical Experimental Design (NED) in this paper. In practice, $Q = kN_p$ simulations (with k a small integer usually equal to 2, 3 or 4) are used.

2.2. Multi-Element Generalized Polynomial Chaos (ME-gPC)

gPC can be interpreted as a polynomial approximation of the QoI depending on ξ. To reduce the approximation error, high polynomial orders may be required. Thus, when the QoI is non linear and the number of uncertain parameters is high, the number of simulations required to calculate the gPC coefficients may be high. Thus, with a high degrees of freedom number DM the calculation cost may be prohibitive. The solution is,therefore, to split ξ into a collection of m non-intersecting elements and to use a low order polynomial approximation on each element. That is basically what the scheme of ME-gPC rely on Wan and Karniadakis (2005).

The local physical variables β_j^k, in each the k^{th} element $\prod_{i=1}^{r}[a_i^k, b_i^k]$, are expressed in terms of independent uniform random variables ξ_j^k in $[-1, 1]^r$ through

$$\beta_j^k = \frac{b_j^k + a_j^k}{2} + \frac{b_j^k - a_j^k}{2}\xi_j^k. \tag{4}$$

Consequently, the Legendre polynomials can be exploited.

The gPC can be used locally as follows :

$$X_k(\bar{\xi}^k) \approx \sum_{j=0}^{N_p} \bar{x}_{k,j} \phi_j(\bar{\xi}^k). \tag{5}$$

where $X_k(\bar{\xi}^k)$ is the random process corresponding to the k^{th} element.

The local mean $\hat{X}_{p,k}$ and variance $\sigma^2_{p,k}$ approximated in the k^{th} element by the gPC with order p are:

$$\begin{cases} \hat{X}_{p,k} = \bar{x}_{k,0} \\ \sigma^2_{p,k} = \dfrac{1}{2^r} \displaystyle\sum_{j=1}^{N_p} \bar{x}^2_{k,j} \langle \phi^2_j \rangle. \end{cases} \tag{6}$$

Several criteria have been proposed in the literature for the convergence of the ME-gPC algorithm and they depend on the aim of using the ME-gPC. For this study, the criteria are presented in the next section.

3. ME-gPC to locate a discontinuity in the quantity of interest

3.1. Algorithm

In this section, a method based on ME-gPC to locate a discontinuity in a quantity of Interest (QoI) derived from a deterministic model (DM) of a mechanical system is proposed. The goal is not to obtain an accurate representation of the QoI but to be able to locate the discontinuity, i.e. to know the values of the uncertain parameters for which the discontinuity appears.

The idea of the method is based on the fact that a QoI that contains a discontinuity has a high variance compared to a QoI that does not contain discontinuity. The use of gPC to estimate the variance of the QoI is justified by the fact that the variance of a gPC expansion is estimated directly from the chaos coefficients (Eq. (6)) without the need for additional calculations. Moreover, the method consists to determinate the QoI with a low order polynomials in the ME-gPC representation (in this paper, $p = 1, 2$ *and* 3). Then, it is assumed that if the discontinuity is in the given element of the stochastic parameters space, the ME-gPC expansion has a large value of the variance.

From these considerations a ME-gPC algorithm is built, in which at each step and for each element the variance $\sigma^2_{p,k}$, computed directly from the gPC coefficients using Eq. (6), is compared to a threshold θ_1. Then, if for a given element k

$$\sigma^2_{p,k} \geq \theta_1, \tag{7}$$

it is assumed that the discontinuity is in the element. The latter is divided by two in each direction of the stochastic space in order to identify more accurately the localization of the discontinuity. On the contrary, if the condition Eq. (7) is not satisfy the element k is supposed not to contain a discontinuity, this information is save and the element is removed from the algorithm.

θ_1 is choosed so that the variance of the element which contains the discontinuity always satisfy the condition Eq. (7). Therefore, two other criteria to stop the algorithm are introduced. The first is based on the element size. Thus, after defining the minimum element size $J_{\min}$ as follows

$$J_{\min} = \theta_2 J_0 \tag{8}$$

where J_0 is the size of the initial element corresponding to the stochastic parameters space and θ_2 is a percentage. The element is actually divided into two equal parts in each direction of the stochastic space if the following condition

$$J_i \geq J_{\min} \tag{9}$$

holds, where J_i represents the size of the elements at a given iteration i, it is the same for all elements because at each iteration the division is performed in each direction of the stochastic. If conditions (9) does not hold the algorithm is stopped and we assume that the discontinuity in the QoI profile is in remaining elements.

In Sect. 6, a comparison is performed with a reference method which needs N simulations of the DM to locate a discontinuity in the QoI profile. Therefore, the proposed method is effective if the number of numerical simulations N' required to obtain the gPC coefficients in all elements is smaller than N. Consequently, N' should verify

$$N' \leq N. \tag{10}$$

Otherwise the algorithm is stopped and, in general, the discontinuity in the QoI profile has not been located.

The algorithm is summarized in Fig. 1. At the first step, only one element is present (i.e. the whole stochastic parameter space) and for a given iteration the parameter space has been divided into K elements during the previous iterations. At each iteration, the gPC coefficients are computed for the K elements and we check if the computational cost of this is larger than the one of the reference (Eq. (10)). If that is the case the algorithm is stopped and in general the discontinuity in the QoI profile has not been located. If Eq. (10) holds, we check the variance of each of the K elements (Eq (8)). If it is smaller than the threshold θ_1, the element is removed from the algorithm. If it is larger, it is kept and K' elements remain at the exit of the loop in k. If Eq. (9) does not hold, the algorithm is stopped and we assume that the discontinuity in the QoI profile is in the K' remaining elements. If Eq. (9) holds, then each of the K' elements is divided into two in each direction of the stochastic parameters space, then a new iteration begins with $K = 2^r K'$.

3.2. The Numerical Experimental Design (NED)

In the context of the ME-gPC method mQ is the maximum necessary number of simulations required to built the gPC coefficients in the case of m elements. In practice it is possible to reduce this number. Indeed, the points used to calculate the gPC coefficients of an element at the i^{th} iteration can be used to estimate the gPC coefficients for the elements of the $(i+1)^{th}$ iteration generated from the split of the element of the i^{th} iteration. The set of points at $(i+1)^{th}$ iteration for an element therefore is equal to $Q' = Q_{inherited} + Q_{added}$ where $Q_{inherited}$ is the number of inherited points from the i^{th} iteration and which belong to the considered element and Q_{added} is new set of points

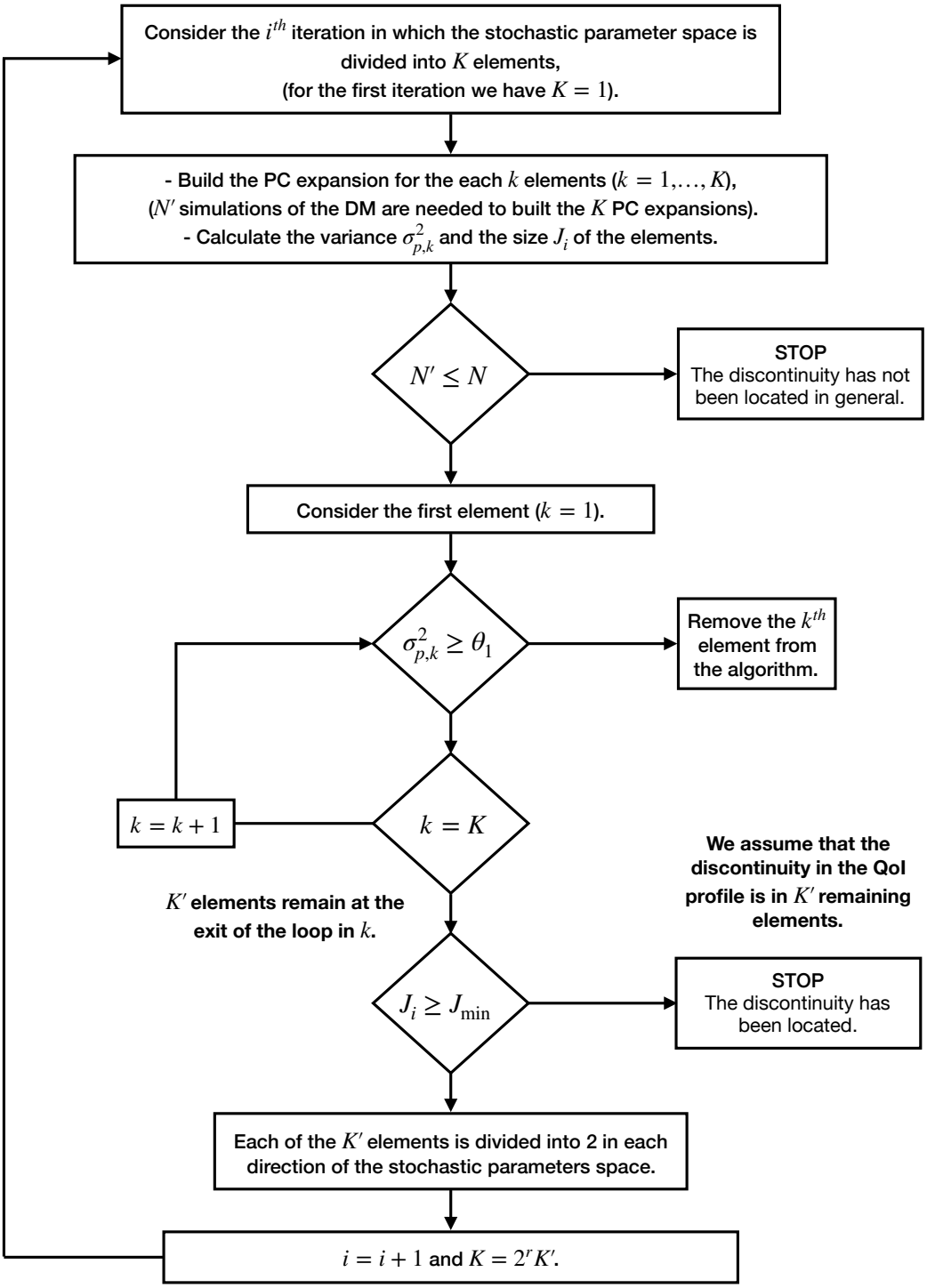

Figure 1: Algorithm of the proposed method based on the ME-gPC.

generated $Q_{added} < Q$. Thus, the number of simulations is equal to the sum of the added points for all elements.

The method is illustrated in Fig. 2 for $r = 1$, $p = 1$ and $k = 2$ ($N_p = 2$, $Q = 4$). In this work, the NED is built by this method.

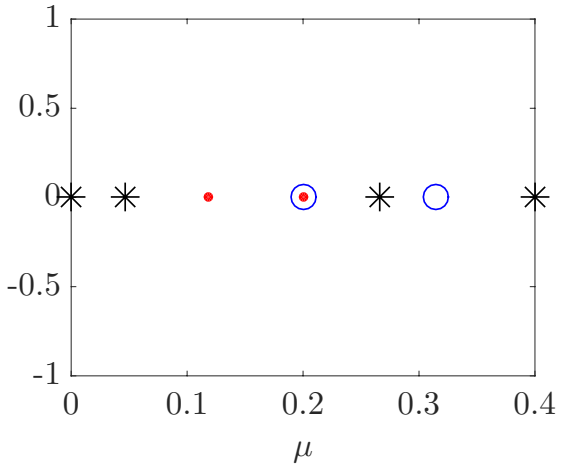

Figure 2: Mapping the LHS sample to the design space in iteration 2 with $r = 1$, $p = 1$, $k = 2$ and $Q = 4$. ($*$) Inherited points from the element [0 , 0.4] of the iteration 1. ($\bullet$) New LHS points at the first element [0 , 0.2] of the iteration 2. ($\bigcirc$) New LHS points at the second element [0.2 , 0.4] of the iteration 2.

4. System under study

4.1. The primary system

The well-known two degree-of-freedom (DOF) Hultèn's analytical model (Hultén (1997, 1993)) is used in this paper. This phenomenological simple model is able to reproduce the typical behavior of friction system, especially the mode-coupling phenomenon. The model is composed of a mass m held against a moving strip. The contact between the mass and the strip is modeled by two plates supported by two different springs each comprising a linear component (k_1 and k_2), and a cubic component (k_1^{NL} and k_2^{NL}) as shown in Fig. 3. Damping is integrated as indicated in Fig. 3 introducing the damping coefficients c_1 and c_2. It is assumed that there is always sliding contact between the mass and the strip. The friction coefficient is assumed to be constant and the strip moves at a constant velocity. The direction of friction force is assumed to do not change because the relative velocity between the strip speed and dx_1/dt or dx_2/dt is supposed to be positive. The Coulomb's law is assumed for the description of the friction contact: the tangential friction force F_T is proportional to the normal force F_N, i.e. $F_T = \mu F_N$, where μ is the friction coefficient. The equations of motion can be written as follows

$$m\frac{d^2x_1}{dt^2} + c_1\frac{dx_1}{dt} + k_1x_1 - \mu k_2x_2 + k_1^{NL}x_1^3 - \mu k_2^{NL}x_2^3 = 0 \tag{11a}$$

$$m\frac{d^2x_2}{dt^2} + c_2\frac{dx_2}{dt} + k_2x_2 + \mu k_1x_1 + \mu k_1^{NL}x_1^3 + k_2^{NL}x_2^3 = 0. \tag{11b}$$

Eq. (11) which is defined as the primary system in this study.

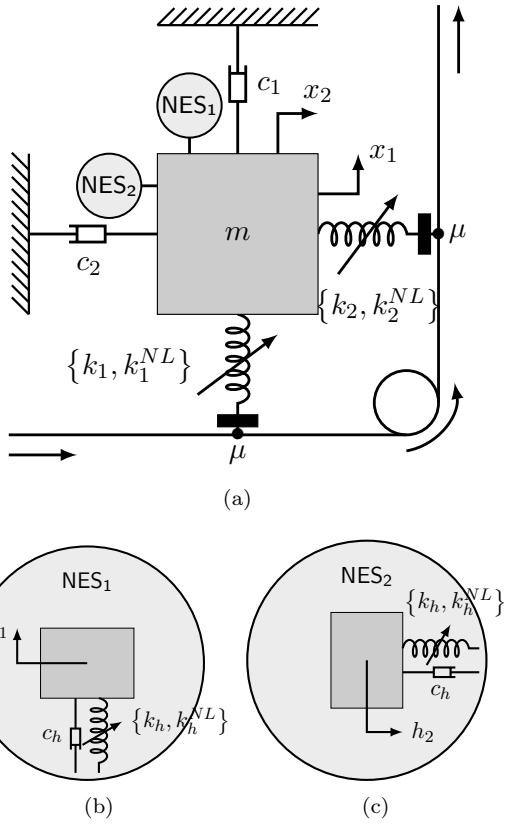

Figure 3: The mechanical model. (a) Mechanical system with NESs; (b) Zoom on the NES$_1$; (c) Zoom on the NES$_2$.

4.2. Mechanical model with Nonlinear Energy Sinks

Two strongly cubic and identical NESs with masses m_h in kg, damping coefficients c_h and a cubic stiffness k_h^{NL}, are attached on the primary system in an ungrounded configuration (see Fig. 3).

Introducing the NESs displacements $h_1(t)$ and $h_2(t)$ in Eq. (11), the equations of motion of the coupled system are

$$\frac{d^2x_1}{dt^2} + \eta_1\omega_1\frac{dx_1}{dt} + \omega_1^2x_1 - \mu\omega_2^2x_2 + \varphi_1x_1^3 - \mu\varphi_2x_2^3 + \eta_h\omega_1\left(\frac{dx_1}{dt} - \frac{dh_1}{dt}\right) + \xi_h\left(x_1 - h_1\right) + \varphi_h\left(x_1 - h_1\right)^3 = 0 \tag{12a}$$

$$\epsilon\frac{d^2h_1}{dt^2} + \eta_h\omega_1\left(\frac{dh_1}{dt} - \frac{dx_1}{dt}\right) + \xi_h\left(h_1 - x_1\right) + \varphi_h\left(h_1 - x_1\right)^3 = 0 \tag{12b}$$

$$\frac{d^2x_2}{dt^2} + \eta_2\omega_2\frac{dx_2}{dt} + \omega_2^2x_2 + \mu\omega_1^2x_1 + \mu\varphi_1x_1^3 + \varphi_2x_2^3 + \eta_h\omega_1\left(\frac{dx_2}{dt} - \frac{dh_2}{dt}\right) + \xi_h\left(x_2 - h_2\right)^+ \varphi_h\left(x_2 - h_2\right)^3 = 0 \tag{12c}$$

$$\epsilon\frac{d^2h_2}{dt^2} + \eta_h\omega_1\left(\frac{dh_2}{dt} - \frac{dx_2}{dt}\right) + \xi_h\left(h_2 - x_2\right) + \varphi_h\left(h_2 - x_2\right)^3 = 0, \tag{12d}$$

where the following notation has been introduced: the relative damping coefficient $\eta_i = c_i/\sqrt{mk_i}$, the natural pulsations $\omega_i = \sqrt{k_i/m}$, $\varphi_i = k_i^{NL}/m$ (with $i = 1, 2$), $\epsilon = m_h/m$, $\xi_h = k_h/m$, $\eta_h = c_h/\sqrt{mk_1}$ and $\varphi_h = k_h^{NL}/m$. Because strongly cubic NESs are assumed $k_h \ll \varphi_h$. In theoretical and experimental works studying systems with NESs, the mass ratio ϵ is in general in a range 0.01-0.1 and this convention will be followed in current work.

5. Preliminary results: vibratory levels and possible steady-state regimes

In this section, the role of the NESs attachments to control the amplitudes of the LCOs is presented. Bergeot et al. (2017b) have been shown that, as usual in the context of LCOs mitigation by means of NES, four main types of steady-state regimes generated when two NESs is attached on the primary system: complete suppression of the instability, mitigation through Periodic Response (PR), mitigation through Strongly Modulated Response (SMR) or no mitigation.

An illustration of these different steady-state regimes is presented in Fig. 4 which shows the displacements $x_1(t)$ with respect to times with and without the NESs attachments. The regimes described above are classified into two categories depending on whether the NESs act or not and therefore if the instability is mitigated or not. The first ones are mitigated regimes which group the complete suppression (see. Fig. 4(a)), PR (see. Fig. 4(b)) and SMR (see. Fig. 4(c)) regimes. The second is the no mitigation (see. Fig. 4(d)) regime.

In the studies presented in the following sections the QoI under consideration is the amplitude of the variables x_1 in the system with NES (Eq. (12)) and within steady-state regime, it is denoted $A_{x_1}^{wNES}$ and defined as follows

$$A_1^{wNES} = \frac{\max\left[x_1^{SSR}(t)\right] - \min\left[x_1^{SSR}(t)\right]}{2}, \tag{13}$$

where $x_1^{SSR}(t)$ is the times series of the variables x_1 obtained from the numerical integration of the coupled system (Eq. (12)) within the steady-state regime. For comparison the amplitude A_1^{woNES} corresponding to the system without NES (see Eq. (11)) is also defined.

In practice, the time integration of the system ((12) resp. (11)) is done between $t_b = 0$ and $t_e = 4$ seconds and the amplitude A_1^{wNES} (resp. A_1^{woNES}) is computed in the interval $[0.9t_e\ t_e]$ in which we assume that the system has reached its steady-state regime.

The amplitudes A_1^{wNES} and A_1^{woNES} are plotted as a function of the friction coefficient μ in Fig. 5 for the following set of parameters

$$\omega_1 = 2\pi 100\ (\text{rad}\cdot\text{s}^{-1}), \tag{14a}$$
$$\omega_2 = 2\pi 85\ (\text{rad}\cdot\text{s}^{-1}), \tag{14b}$$
$$\eta_1 = 0.02, \tag{14c}$$
$$\eta_2 = 0.06, \tag{14d}$$
$$\varphi_1 = 10^5\ (\text{N}\cdot\text{kg}^{-1}\cdot\text{m}^{-3}), \tag{14e}$$
$$\varphi_2 = 0\ (\text{N}\cdot\text{kg}^{-1}\cdot\text{m}^{-3}), \tag{14f}$$
$$\epsilon = 0.05, \tag{14g}$$
$$\xi_h = 0.001\ (\text{N}\cdot\text{kg}^{-1}\cdot\text{m}^{-1}), \tag{14h}$$
$$\eta_h = 0.02, \tag{14i}$$
$$\varphi_h = 1.4\cdot 10^5\ (\text{N}\cdot\text{kg}^{-1}\cdot\text{m}^{-3}). \tag{14j}$$

The figure shows clearly the four steady-state regimes described in the last section and highlight a jump (or discontinuity) in the amplitude profile A_1^{wNES}. This discontinuity corresponds, when μ increases, to the transition from SMR to no suppression regime and separates mitigated regimes and unmitigated regimes. The mitigation limit of the friction parameter is denoted by μ_{ml}, this is the value of μ at the jump.

The following section is devoted to the determination of the mitigation limit considering that two parameters of the model can be uncertain : μ the friction coefficient and η_1 the damping coefficient in the direction x_1. To achieve that, A_1^{wNES} is described using ME-gPC and then, because A_1^{wNES} can have a discontinuity in its profile, the method described in Sect. 3 is used.

6. Application and results

In this section, the method presented in Sect. 3 is applied to locate the discontinuity in the steady-state amplitude profile A_1^{wNES} (see Eq. (13) and Fig. 5) of the system under study Eq. (12). Then the Propensity of the system to undergo a Harmless Steady-State Regime (PHSSR), defined below, is computed. Finally, for validation purposes, the method is compared to a reference method.

The uncertain parameters are supposed to be driven by a uniform distribution law. Two parameters are assumed to be uncertain: the friction coefficient μ and the damping coefficient η_1. First only μ is considered uncertain and then both of the parameters are supposed to be uncertain.

6.1. Propensity to undergo Harmless Steady-State Regimes

The discontinuity in the A_1^{wNES} profile is located in the uncertain parameters space V and then the part of V in which the steady-state regimes are harmless is denoted V_H. The system is in a harmless steady-state regime if it is not in a *no suppression* regime (see Sect. 5), i.e.

- it would be stable even without the NESs, or
- it is in *complete suppression* regime, or
- it is in mitigated regime (PR or SMR).

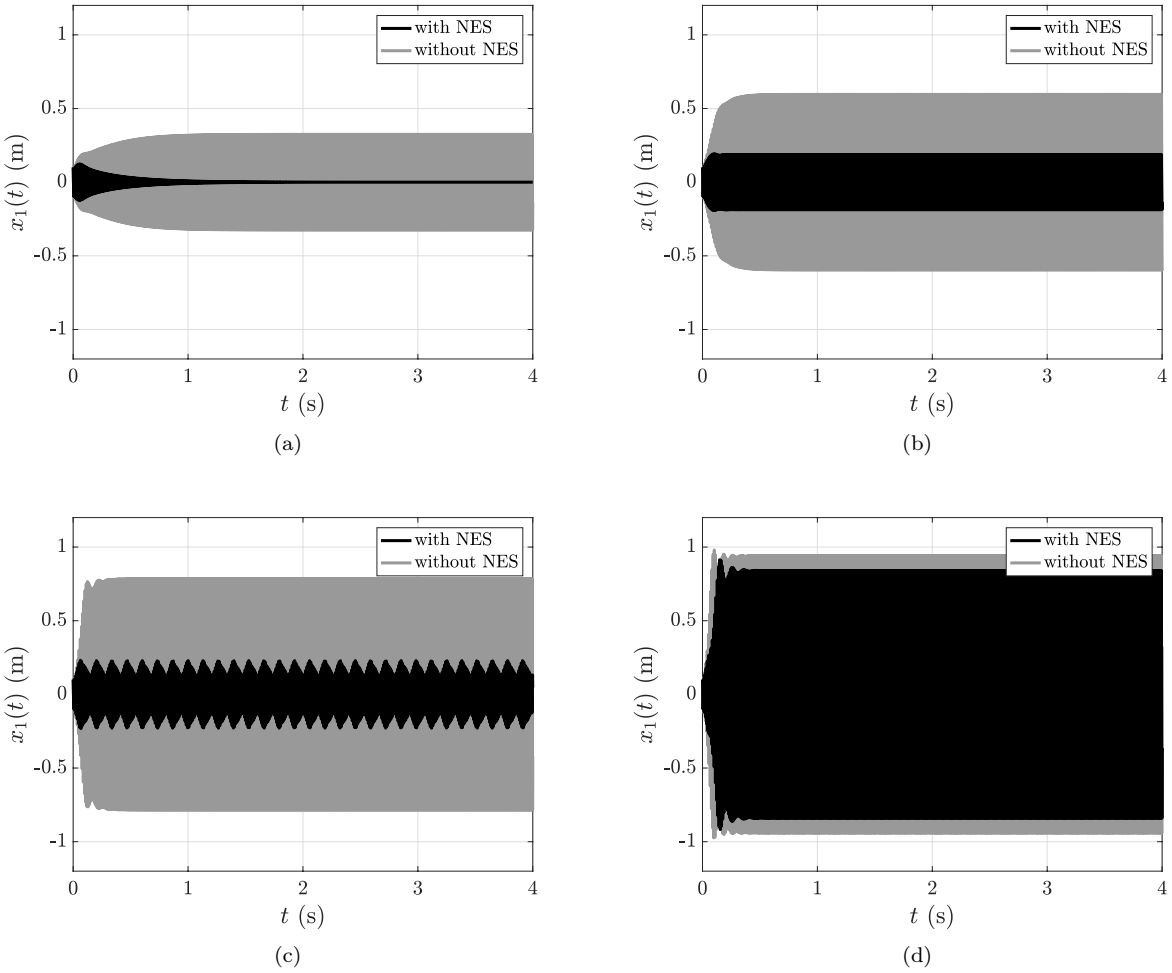

Figure 4: Comparison between time serie $x_1(t)$ resulting from the numerical integration of the friction system with and without NESs. (a) Complete suppression, $\mu = 0.16$; (b) Mitigation: PR, $\mu = 0.18$; (c) Mitigation: SMR, $\mu = 0.2$; (d) No mitigation, $\mu = 0.22$. The set of parameters Eq. (14) is used.

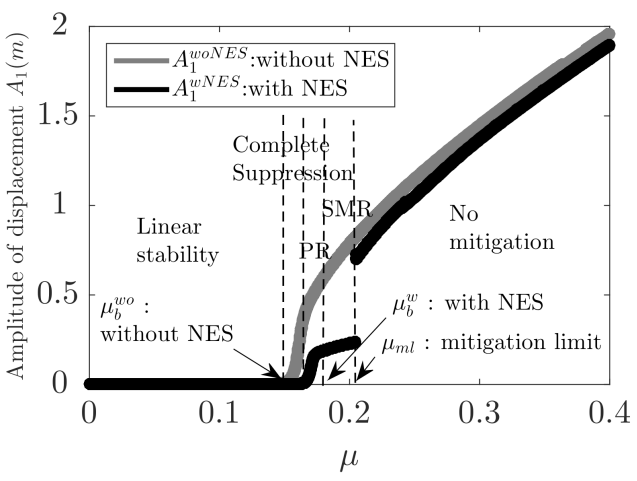

Figure 5: Amplitudes A_1^{wNES} and A_1^{woNES} as a function of the friction coefficient μ. The set of parameters Eq. (14) is used.

In Fig. 5, all the steady-state regimes situated on the left of the mitigation limit μ_{ml} are harmless.

Generally, if $\beta = (\beta_1, ..., \beta_r)$ is the vector of r uncertain physical parameters under consideration and $f(\beta)$ the associated probability density function. Then, the PHSSR is defined as follows

$$\text{PHSSR} = \int_{V_H} f(\beta) d\beta, \tag{15}$$

which becomes for uniformly distributed parameters within the space $\prod_{i=1}^{r}[a_i, b_i]$

$$\text{PHSSR} = \int_{V_H} \frac{1}{\prod_{i=1}^{r}(b_i - a_i)} d\beta. \tag{16}$$

In the next sections, the results are presented in terms of computational cost on the one hand and in terms of accuracy compared to the reference method on the other hand. To this end, some quantities are introduced for each simulation:

- the ratio $\theta_1/(\text{Max}_{\text{Ref}} - \text{Min}_{\text{Ref}})$ to know how much the variance criterion θ_1 varies compared to the reference (Max_{Ref} and Min_{Ref} represent respectively the maximum and the minimum of the amplitude found by the reference method).
- the number of simulations to estimate the computational cost of the method.
- the PHSSR value from the method estimated using the upper bounds of the last intervals find by the algorithm presented in Fig. 1.
- the relative error E_{PHSSR} of the PHSSR obtained with the presented ME-gPC based method ($\text{PHSSR}_{\text{ME-gPC}}$) and the PHSSR obtained with the reference method ($\text{PHSSR}_{\text{Ref}}$), it is defined as follows

$$E_{\text{PHSSR}} = \frac{|\text{PHSSR}_{\text{ME-gPC}} - \text{PHSSR}_{\text{Ref}}|}{\text{PHSSR}_{\text{Ref}}} \times 100. \quad (17)$$

In the case with one uncertain parameter, the last interval found the algorithm of the method is denoted $I_{ml} = [\mu_1, \mu_2]$. This interval contains the jump (i.e. $\mu_{ml} \in I_{ml}$). Then, the midpoint μ_{mid} of the interval is calculated giving two criteria. The first is the relative error E between the midpoint of the interval and reference value of the mitigation limit found by the reference:

$$E = \frac{|\mu_{\text{mid}} - \mu_{ml}^{\text{Ref}}|}{\mu_{ml}^{\text{Ref}}} \times 100 \quad (18)$$

where μ_{ml}^{Ref} is the mitigation limit found by the reference method. The second is the relative difference D between the midpoint and the bounds of the interval:

$$D = \frac{|\mu_1 - \mu_{\text{mid}}|}{\mu_{\text{mid}}} \times 100. \quad (19)$$

In the case of two uncertain parameters, when the algorithm stopped several subplanes $[\mu_1^{(k)}, \mu_2^{(k)}] \times [\eta_{1_1}^{(k)}, \eta_{1_2}^{(k)}]$ (with $k = 1, \ldots, K$) containing the discontinuity frontier are found (see black line in Fig. 8). The relative differences D_μ and D_{η_1} between the midpoints μ_{mid} and $\eta_{1\text{mid}}$ in each direction and the corresponding bounds are computed as

$$D_\mu = \frac{\left|\mu_1^{(k)} - \mu_{\text{mid}}^{(k)}\right|}{\mu_{\text{mid}}^{(k)}} \times 100, \quad (k = 1, \ldots, K) \quad (20)$$

and

$$D_{\eta_1} = \frac{\left|\eta_{1_1}^{(i)} - \eta_{1\text{mid}}^{(i)}\right|}{\eta_{1\text{mid}}^{(i)}} \times 100, \quad (k = 1, \ldots, K). \quad (21)$$

Note that because in each direction for all $k = 1, \cdots, K$, $\mu_1^{(k)} - \mu_{\text{mid}}^{(k)}$ and $\eta_{1_1}^{(i)} - \eta_{1\text{mid}}^{(i)}$ are constant, D_μ and D_{η_1} are also constant.

6.2. One uncertain parameter: the friction coefficient μ

In this section only the friction coefficient μ is uncertain and it is assumed that it lies within the interval $[a, b] = [0, 0.4]$.

6.2.1. Reference study

As a reference, the DM is simulated for $N = 100$ linearly increasing values of μ from 0 to 0.4 and considering the set of parameters. (14). The interval of μ for which a jump in the amplitude profile is observed is located and we define the mitigation limit as the upper bound of the interval. In this case, the mitigation limit is $\mu_{ml} = 0.2061$ leading, through (16), to a PHSSR equals to 51.52%.

6.2.2. Results

Now the method presented in Sect. 3 is used to estimate the mitigation limit and the PHSSR. The QoI (A_1^{wNES}) estimated by the ME-gPC based method is built through the procedure presented in Sect. 2.2.

First, Fig. 6 shows the successive iterations of the proposed algorithm (see Fig. 1), the gPC order is $p = 1$ and the following criteria are used: $\theta_1 = 0.7 \cdot 10^{-3}$ and $\theta_2 = 1\%$. The curve in black is the amplitude obtained by the reference and the color curves are the amplitude obtained from the gPC in each of the K elements of the considered iteration. At the first iteration (Fig. 6(a)) we have only one element and, because Eqs. (7)-(9)-(10) hold, it is divided into two parts shown in Fig. 6(b). In the latter, Eqs. (7)-(9)-(10) hold again in both elements and therefore they are divided and we move to the third iteration (Fig. 6(c)). At this iteration the variance of the leftmost element does not satisfy Eq. (7) and it is therefore removed from the algorithm and the corresponding amplitude is not depicted on the figure. The three other elements are divided into two parts and we move to next iteration and so on until the algorithm stops the eighth iteration because Eq. (9) is not satisfied anymore. We assume that the mitigation limit μ_{ml} is within the last element in which the amplitude is depicted in orange in Fig. 6(h).

Then, in order to find the right combination between the values of the different criteria and the computational cost, several simulations have been made with different value of θ_1 and of the order p of the gPC. The NED is built each time according to the method described in Sect. 3.2.

The results are presented in Tab. 1 which shows the comparison between the reference and the proposed method for $\theta_2 = 1\%$, $p = 1, 2$ and 3 and for different value of the criterion θ_1.

Because the algorithm of the ME-gPC based method is always stopped due to the criterion θ_2, the width of the last interval I_{ml} is the same whatever the value of the criterion θ_1 and of the gPC order p. The last interval found is $I_{ml} = [0.2031, 0.2063]$ that it can be defined also as $I_{ml} = 0.2047 \pm 0.78\%$. The size of this interval represent 0.8% of the main interval. It is well below $\theta_2 = 1\%$. The midpoint value is compared with the mitigation limit found by the reference

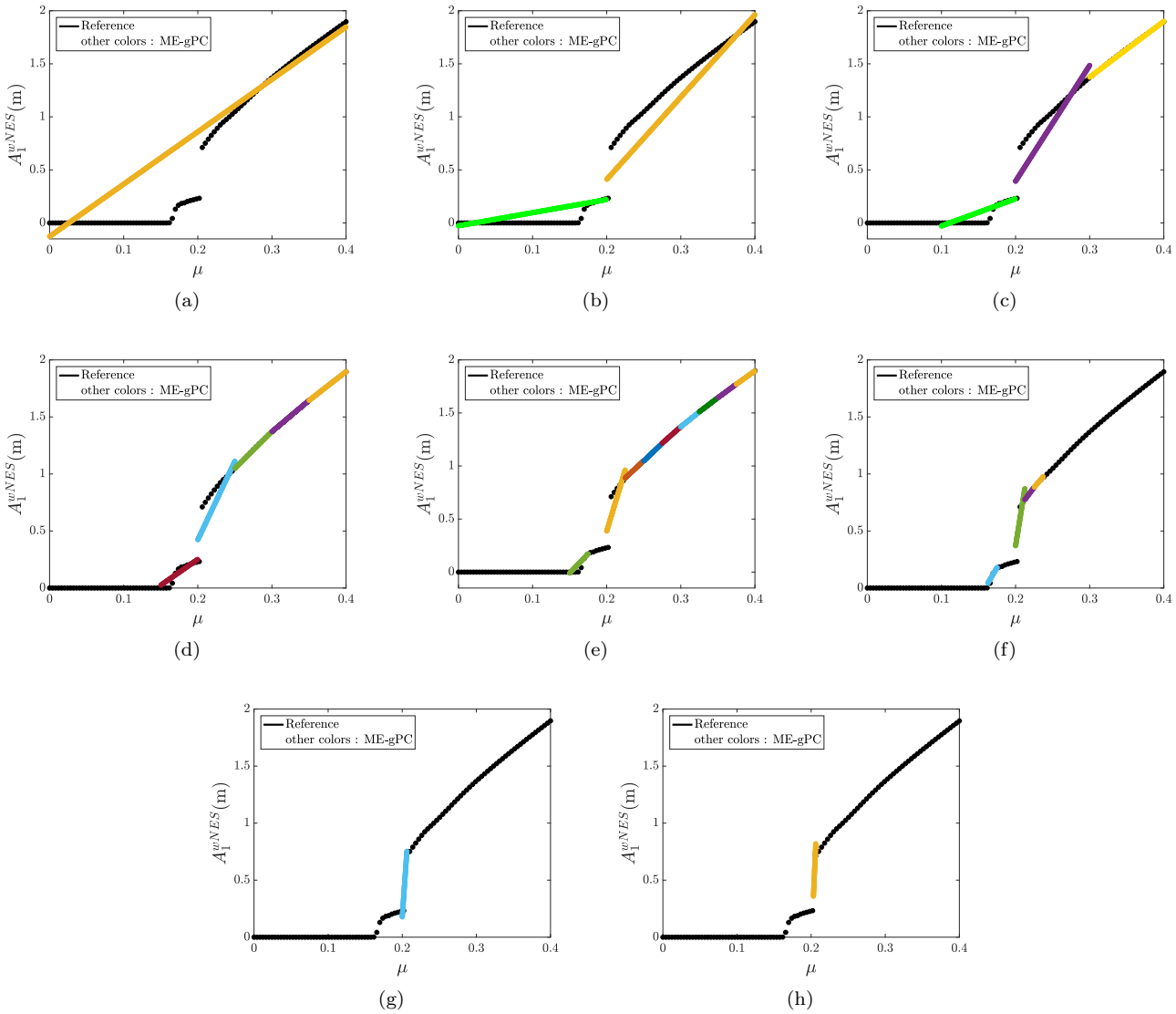

Figure 6: The evolution of the decomposition algorithm. The friction coefficient μ is uncertain, $\theta_1 = 0.7 \cdot 10^{-3}$, $\theta_2 = 1\%$ and $p = 1$. (a) Iteration 1; (b) Iteration 2; (c) Iteration 3; (d) Iteration 4; (e) Iteration 5; (f) Iteration 6; (g) Iteration 7; (h) Iteration 8.

method, the relative error is equal to 0.44%. The PHSSR is equal to 51.57% which leads to a relative error compared with the reference method equals to 0.68%. Note that when the $N' = 100$ the algorithm is stopped because of (10) and the mitigation limit is not located.

For all the cases, the maximum value of the variance criterion θ_1 represents the value which corresponds to a change of criteria that stops the algorithm (i.e. after this value, the criterion θ_1 starts to stop the algorithm). This value is the optimal because it corresponds to the smallest possible value of the number of simulations to locate the mitigation limit. According to these last values ($\theta_1 = 17 \cdot 10^{-3}$ for $p = 1$, $\theta_1 = 0.9 \cdot 10^{-3}$ for $p = 2$ and $\theta_1 = 0.4 \cdot 10^{-3}$ for $p = 3$), the number of simulations is lower when $p = 1$ than in the case when $p = 2$ and $p = 3$ and the PHSSR remains constant because the intervals I_{ml} are the same for each case.

In order to obtain a reduced calculation cost, it is possible to increase the value of the threshold for second criterion θ_2. For example, in the case that $\theta_2 = 5\%$, the last found interval is $I_{ml} = [0.2, 0.2125]$. The size of the interval increases compared to the case where $\theta_2 = 1\%$ which increases the relative error E_{PHSSR} from 1.21% in the case that $\theta_2 = 1\%$ to 4.25%. The number of simulations reduces and becomes equal to 40 for $\theta_1 = 10 \cdot 10^{-3}$ and $p = 1$.

As a conclusion, the best choice for the value of the gPC order appears to be $p = 1$. Indeed, because the accuracy of the PHSSR prediction is fixed by the choice of the criterion θ_2, the prediction with $p = 1$ is as accurate as for larger order ($p = 2$ or 3) but with a smaller number of simulations.

Table 1: comparison of the results between the reference method and the ME-gPC based method, $\theta_2 = 1\%$ and the parameter μ is uncertain.

		ME-gPC				
Variance criterion $\theta_1(.10^{-3})$	$p=1$	0.7	2	10	15	17
	$p=2$	0.05	0.1	0.5	0.7	0.9
	$p=3$	0.05	0.07	0.1	0.3	0.4
$\frac{\theta_1}{\text{Max}_{\text{Ref}} - \text{Min}_{\text{Ref}}}$ (%)	$p=1$	0.03	0.1	0.52	0.79	0.89
	$p=2$	0.002	0.005	0.02	0.03	0.04
	$p=3$	0.002	0.003	0.005	0.01	0.02
Number of simulations	$p=1$	100	100	52	53	53
	$p=2$	94	79	78	78	71
	$p=3$	100	99	99	89	80
PHSSR (%)	$p=1$					
	$p=2$			51.57		
	$p=3$					
E_{PHSSR} (%)	$p=1$					
	$p=2$			0.097		
	$p=3$					
I_{ml}	$p=1$					
	$p=2$			[0.2031, 0.2063]		
	$p=3$					
μ_{mid}	$p=1$					
	$p=2$			0.2047		
	$p=3$					
E (%)	$p=1$					
	$p=2$			0.68		
	$p=3$					
D (%)	$p=1$					
	$p=2$			0.78		
	$p=3$					

6.3. *Two uncertain parameters: the friction coefficient μ and the damping coefficient η_1*

In this section, the parameter η_1 is also assumed to be uncertain and driven also by an uniform distribution within $[0.1\ ,\ 2.1]$. η_2 is fixed and it is equal to 0.09.

6.3.1. *Reference study*

The reference is obtained in a similar way as in Sect. 6.2.1. The 2-dimensional parameter space is divided into $N = 100 \times 100 = 10000$ squares between $\mu = 0$ and $\mu = 0.4$ and $\eta_1 = 0.1$ and $\eta_1 = 2.1$, again considering the parameters (14), except for η_1 and η_2. Fig. 7 shows a 3D graph containing the $N = 10000$ realizations of the amplitude of displacement A_1^{wNES}, as a function of the two uncertain parameters. The discontinuity in the amplitude surface is visible and allows us to define, as previously in Sect. 6.2.1, the mitigation limit as the projection of it in the (μ, η_1)-plane. This projection is depicted in Fig. 8 together with lines corresponding to the Hopf bifurcation points with and without NESs[1]. The four regimes described in Sect. 5 and depicted in the case with only one uncertain parameter in Fig. 5 are shown here.

[1] As usual, the bifurcation point of the system without NESs (resp. with NESs) are found by looking the sign of the eigenvalues real parts of the system (11) (resp. (12)).

In the (μ, η_1)-plane, the mitigation limit can be defined as the curve $\eta_{1,ml}$ as a function of μ. Then, through (16), we obtain

$$\begin{aligned} \text{PHSSR} &= \int_0^{0.4} \int_{0.1}^{\eta_{1,ml}(\mu)} \frac{1}{0.4 \times 2} d\mu d\eta_1 \\ &= \frac{\int_0^{0.4} [\eta_{1,ml}(\mu) - 0.1]\, d\mu}{0.8}. \end{aligned} \tag{22}$$

The integral in the numerator of (22) is evaluated numerically and we find a PHSSR equal to 92.16%.

6.3.2. *Results*

The evolution of the mitigation limit is now determined by the proposed method in the considered stochastic space. As in the case of one uncertain parameter, the NED is built according to the method described in Sect. 3.2. Overall, the number of simulations needed to obtain the prediction of the PHSSR is logically larger than in the case of a single uncertain parameter.

Tab. 2 shows the comparison with the reference method for $p = 1$, 2 and 3 and for $\theta_2 = 1\%$. The relative differences D_μ and D_{η_1} are equal to 1.2% and 12.45% respectively. As previously, increase the value of θ_1 reduces the number of simulations to reach 2122 simulations when $\theta_1 = 29 \cdot 10^{-3}$ and $p = 1$, 4195 simulations when $\theta_1 = 5 \cdot 10^{-3}$ and $p = 2$ and 7293 simulations where $\theta_1 = 1 \cdot 10^{-3}$ and $p = 3$.

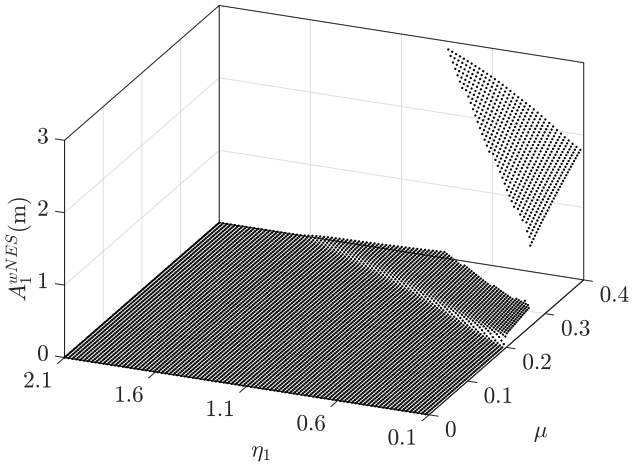

Figure 7: Amplitude A_1^{wNES} as a function of the friction coefficient μ and the damping coefficient η_1. $\omega_1 = 2\pi 100$, $\omega_2 = 2\pi 85$, φ_1 =10 0000, $\varphi_2 = 0$, $\epsilon = 0.05$, $\xi_h = 0.001$, $\eta_h = 0.02$ and $\varphi_h = 140000$.

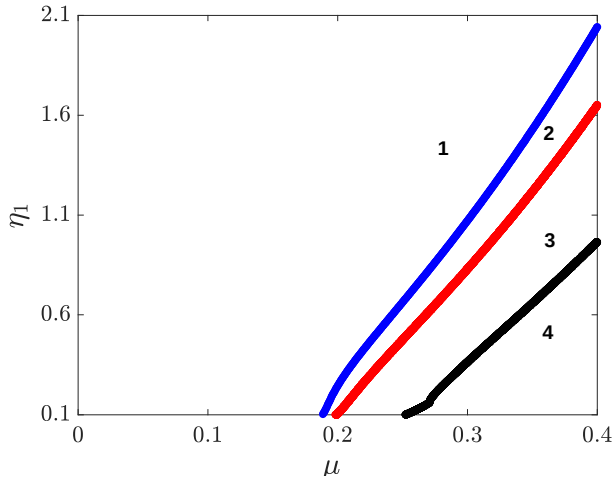

Figure 8: Evolution of the mitigation limit and Hopf bifuraction points with and without NESs using the 10 000 simulations of the reference. (blue line) Hopf Bifurcation point without NES ($\eta_{1_b}^{wo}$); (red line) Hopf Bifurcation point with NES ($\eta_{1_b}^{w}$); (black line) Mitigation limit ($\eta_{1_{ml}}$). 1: Linear stability without NESs; 2: Linear stability with NESs; 3: Mitigated regimes (PR or SMR); 4: No mitigated regimes.

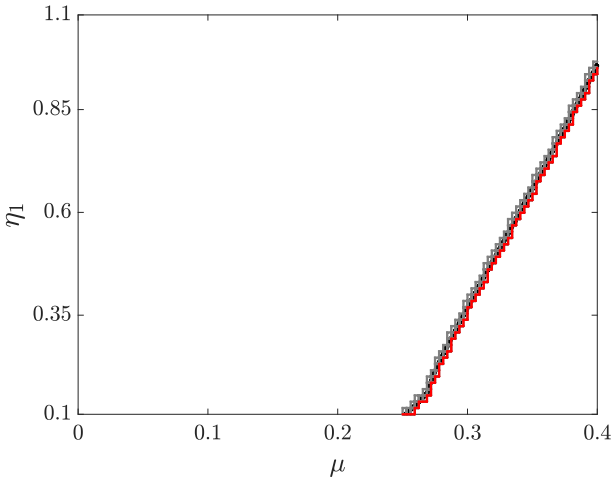

Figure 9: The mitigation limit in the (μ, η_1)-plane. The reference is the black line. The last K' elements which remain at the end of the algorithm presented in Fig. 1 are depicted by gray squares. The left side of the squares (the red line) constitutes the mitigation limit. The parameters μ and η_1 are uncertain , $\theta_1 = 1 \cdot 10^{-3}$, $\theta_2 = 1\%$ and $p = 1$.

Whatever the value of p, the PHSSR, calculated from the lower bounds (the red line in Fig. 9), is equal to 92.39% with a relative error E_{PHSSR} equals to 0.24%.

As an example of the effect of increasing θ_2, results for $\theta_2 = 5\%$ were obtained. Only the main conlculions are here given. The relative error E_{PHSSR} increases compared to the value obtained for $\theta_2 = 1\%$ and it reaches $E_{\text{PHSSR}} = 1.31\%$. The number of simulations decreases and becomes equal to 448 for $\theta_1 = 20 \cdot 10^{-3}$ and $p = 1$.

As a conclusion, $p = 1$ is again the best choice for the gPC order in terms of accuracy and computational cost. The difficulty of the method is to find the value of θ_1 which allows to identify the jump and at the same time to get the number of simulations as low as possible.

7. Conclusion

In the present work, mitigation of friction-induced vibrations in a 2-DOF friction system with uncertain parameters by means of Nonlinear Energy Sinks (NESs) has been considered. In this kind of unstable systems coupled to NESs, a discontinuity is often observed in the evolution of the Limit Cycle Oscillation (LCO) amplitude with respect to a chosen bifurcation parameter. This discontinuity represents the transition from mitigated regimes (called harmless steady-state regimes because having small amplitudes) to unmitigated regimes (with large LCO amplitudes).

The aim was to develop an original method which allows to predict these discontinuities and therefore to estimate the Propensity of the system to undergo a Harmless Steady-State Regime (PHSSR) in taking into account the probability distribution of uncertain bifurcation parameters.

The method is an algorithm based on the Multi-Element generalized Polynomial Chaos (ME-gPC) and consists of dividing, at each iteration, the stochastic parameters space and building a metamodel of the LCO amplitude in each subspace. A variance threshold and an subspace size criterion are used to know in which subspace is the discontinuity and to stop the algorithm respectively. When the algorithm is stopped the discontinuities are localized in the last small subspaces of the stochastic parameters space.

The results can be summarized as follows: firstly, because the objective of this study is to predict the discontinuity and not to obtain an accurate representation of the

Table 2: Comparison of the results between the reference method and the ME-gPC based method, $\theta_2 = 1\%$ and the parameters μ and η_1 are uncertain.

		ME-gPC				
Variance criterion $\theta_1(.10^{-3})$	$p=1$	1	10	20	26	29
	$p=2$	0.8	1	2	4	5
	$p=3$	0.6	0.7	0.8	0.9	1
$\frac{\theta_1}{\text{Max}_{\text{Ref}} - \text{Min}_{\text{Ref}}}(\%)$	$p=1$	0.03	0.34	0.69	0.9	1.01
	$p=2$	0.02	0.03	0.06	0.13	0.20
	$p=3$	0.02	0.02	0.02	0.03	0.03
Number of simulations	$p=1$	3723	2188	2183	2144	2122
	$p=2$	4198	4236	4181	4172	4195
	$p=3$	7168	7214	7239	7164	7293
PHSSR (%)	$p=1$					
	$p=2$			92.39		
	$p=3$					
E_{PHSSR} (%)	$p=1$					
	$p=2$			0.24		
	$p=3$					
D_μ	$p=1$					
	$p=2$			0.61		
	$p=3$					
D_{η_1}	$p=1$					
	$p=2$			6.62		
	$p=3$					

LCO amplitude, a polynomial chaos expansion with an order $p = 1$ must be chosen. Indeed, the prediction with $p = 1$ is as accurate as for larger order ($p = 2$ or 3) but with a smaller number of simulations needed to obtain the prediction (i.e. the computational cost). Secondly, for given value of the subspace size criterion, the variance threshold must be chosen as large as possible to ensure en accurate prediction of the PHSSR with a minimum of computational cost. Finally, decreasing the criterion of the subspace size reduces the relative error of the PHSSR compared to the reference but increase the number of simulations.

As a conclusion, the proposed ME-gPC based method proved its capacity to predict the PHSSR and it is less time consuming than the reference method. There is a good compromise between computational cost and accuracy.

As a perspective of this work, the method could be used associated with optimization tools in a strategy of robust design of dry-friction system attached to several NESs by increasing in parallel the number of uncertain parameters.

References

Bellet, R., Cochelin, B., Herzog, P., Mattei, P.O., 2010. Experimental study of targeted energy transfer from an acoustic system to a nonlinear membrane absorber. Journal of Sound and Vibration 329, 2768–2791.

Bergeot, B., Bellizzi, S., 2018. Asymptotic analysis of passive mitigation of dynamic instability using a nonlinear energy sink network. Nonlinear Dynamics 94, 1501–1522. URL: http://link.springer.com/10.1007/s11071-018-4438-0, doi:10.1007/s11071-018-4438-0.

Bergeot, B., Bellizzi, S., 2019. Steady-state regimes prediction of a multi-degree-of-freedom unstable dynamical system coupled to a set of nonlinear energy sinks. Mechanical Systems and Signal Processing 131, 728–750. URL: https://linkinghub.elsevier.com/retrieve/pii/S0888327019303541, doi:10.1016/j.ymssp.2019.05.045.

Bergeot, B., Bellizzi, S., Cochelin, B., 2016. Analysis of steady-state response regimes of a helicopter ground resonance model including a non-linear energy sink attachment. International Journal of Non-Linear Mechanics 78, 72 – 89. URL: http://www.sciencedirect.com/science/article/pii/S0020746215002000, doi:http://dx.doi.org/10.1016/j.ijnonlinmec.2015.10.006.

Bergeot, B., Bellizzi, S., Cochelin, B., 2017a. Passive suppression of helicopter ground resonance using nonlinear energy sinks attached on the helicopter blades. Journal of Sound and Vibration 392, 41 – 55. URL: http://www.sciencedirect.com/science/article/pii/S0022460X16307994, doi:https://doi.org/10.1016/j.jsv.2016.12.039.

Bergeot, B., Berger, S., Bellizzi, S., 2017b. Mode coupling instability mitigation in friction systems by means of nonlinear energy sinks : numerical highlighting and local stability analysis. Journal of Vibration and Control 24, 3487–3511. doi:10.1177/1077546317707101.

Berveiller, M., Sudret, B., Lemaire, M., 2006. Stochastic finite element: a non intrusive approach by regression. European Journal of Computational Mechanics/Revue Européenne de Mécanique Numérique 15, 81–92.

Boroson, E., Missoum, S., Mattei, P.O., Vergez, C., 2017. Optimization under uncertainty of parallel nonlinear energy sinks. Journal of Sound and Vibration 394, 451–464. URL: http://linkinghub.elsevier.com/retrieve/pii/S0022460X16308045, doi:10.1016/j.jsv.2016.12.043.

Cameron, R., Martin, W., 1947. The orthogonal development of nonlinear functionals in series of fourier-hermite functionals. Annals of Mathematics 48, 385–392. doi:http://dx.doi.org/10.2307/1969178.

Cataldo, E., Bellizzi, S., Sampaio, R., 2013. Free vibrations of an uncertain energy pumping system. Journal of Sound and Vibration 332, 6815–6828. doi:10.1016/j.jsv.2013.08.022.

Chevennement-Roux, C., Dreher, T., Alliot, P., Aubry, E., Lainé, J.P., Jézéquel, L., 2007. Flexible Wiper System Dynamic Instabilities: Modelling and Experimental Validation. Experimental Mechanics 47, 201–210. URL: http://link.springer.com/10.1007/s11340-006-9027-3, doi:10.1007/s11340-006-9027-3.

D'Souza, A., Dweib, A., 1990. Self-excited vibrations induced by dry friction, part 2: Stability and limit-cycle analysis. Journal of Sound and Vibration 137, 177–190. URL: http://www.sciencedirect.com/science/article/pii/0022460X9090787Z, doi:10.1016/0022-460X(90)90787-Z.

Eriksson, M., Jacobson, S., 2001. Friction behaviour and squeal generation of disc brakes at low speeds. Proceedings of the Institution of Mechanical Engineers, Part D: Journal of Automobile Engineering 215, 1245–1256. URL: http://dx.doi.org/10.1243/0954407011528789, doi:10.1243/0954407011528789.

Fishman, G.S., 1996. Monte carlo: concepts, algorithms, and applications. Springer Series in Operations Research, Springer, New York. URL: http://cds.cern.ch/record/1614885.

Fritz, G., Sinou, J.J., Duffal, J.M., Jézéquel, L., 2007. Investigation of the relationship between damping and mode-coupling patterns in case of brake squeal. Journal of Sound and Vibration 307, 591–609. doi:10.1016/j.jsv.2007.06.041.

Gendelman, O., Vakakis, A., Bergman, L., McFarland, D., 2010. Asymptotic analysis of passive nonlinear suppression of aeroelastic instabilities of a rigid wing in subsonic flow. SIAM Journal on Applied Mathematics 70, 1655–1677. doi:10.1137/090754819.

Gendelman, O.V., 2012. Analytic treatment of a system with a vibro-impact nonlinear energy sink. Journal of Sound and Vibration 331, 4599–4608. URL: http://dx.doi.org/10.1016/j.jsv.2012.05.021, doi:10.1016/j.jsv.2012.05.021.

Gendelman, O.V., Bar, T., 2010. Bifurcations of self-excitation regimes in a Van der Pol oscillator with a nonlinear energy sink. Physica D 239, 220–229. doi:10.1016/j.physd.2009.10.020.

Gourdon, E., Lamarque, C.H., 2006. Nonlinear energy sink with uncertain parameters. Journal of computational and nonlinear dynamics 1, 187–195.

Guerine, A., Hami, A.E., Walha, L., Fakhfakh, T., Haddar, M., 2016. A polynomial chaos method for the analysis of the dynamic behavior of uncertain gear friction system. European Journal of Mechanics - A/Solids 59, 76 – 84. URL: http://www.sciencedirect.com/science/article/pii/S0997753816300250, doi:https://doi.org/10.1016/j.euromechsol.2016.03.007.

Hoffmann, N., Gaul, L., 2003. Effects of damping on mode-coupling instability in friction induced oscillations. {ZAMM} - Journal of Applied Mathematics and Mechanics / Zeitschrift für Angewandte Mathematik und Mechanik 83, 524–534. URL: http://onlinelibrary.wiley.com/doi/10.1002/zamm.200310022/abstract, doi:10.1002/zamm.200310022.

Hultén, J., 1993. Brake squeal - a self-exciting mechanism with constant friction, in: SAE Truck and Bus Meeting, Detroit, Mi, USA.

Hultén, J., 1997. Friction phenomena related to drum brake squeal instabilities, in: ASME Design Engineering Technical Conferences, Sacramento, CA.

Kinkaid, N., O'Reilly, O., Papadopoulos, P., 2003. Automotive disc brake squeal. Journal of Sound and Vibration 267, 105 – 166. URL: http://www.sciencedirect.com/science/article/pii/S0022460X02015730, doi:https://doi.org/10.1016/S0022-460X(02)01573-0.

Lamarque, C.H., Gendelman, O.V., Ture Savadkoohi, A., Etcheverria, E., 2011. Targeted energy transfer in mechanical systems by means of non-smooth nonlinear energy sink. Acta Mechanica 221, 175. URL: https://doi.org/10.1007/s00707-011-0492-0, doi:10.1007/s00707-011-0492-0.

Lee, Y.S., Vakakis, A.F., Bergman, L.A., McFarland, D.M., 2006. Suppression of limit cycle oscillations in the van der Pol oscillator by means of passive non-linear energy sinks. Structural Control and Health Monitoring 13, 41–75. doi:10.1002/stc.143.

Lee, Y.S., Vakakis, A.F., Bergman, L.A., McFarland, D.M., Kerschen, G., 2007a. Suppression aeroelastic instability using broadband passive targeted energy transfers, part 1: Theory. AIAA Journal 45, 693–711. doi:10.2514/1.24062.

Lee, Y.S., Vakakis, A.F., Bergman, L.A., McFarland, D.M., Kerschen, G., 2007b. Suppression aeroelastic instability using broadband passive targeted energy transfers, part 2: Experiments. AIAA Journal 45, 2391–2400. doi:10.2514/1.24062.

Lee, Y.S., Vakakis, A.F., Bergman, L.A., McFarland, D.M., Kerschen, G., Nucera, F., Tsakirtzis, S., Panagopoulos, P.N., 2008. Passive non-linear targeted energy transfer and its applications to vibration absorption: A review. Proceedings of the Institution of Mechanical Engineers, Part K: Journal of Multi-body Dynamics 222, 77–134. doi:https://doi.org/10.1243/14644193JMBD118.

Lü, H., Yu, D., 2014. Brake squeal reduction of vehicle disc brake system with interval parameters by uncertain optimization. Journal of Sound and Vibration 333, 7313 – 7325. URL: http://www.sciencedirect.com/science/article/pii/S0022460X14006993, doi:https://doi.org/10.1016/j.jsv.2014.08.027.

McKay, M., Beckman, R., Conover, W., 1979. A comparison of three methods for selecting values of input variables in the analysis of output from a computer code. Technometrics 21, 239–245. URL: http://www.jstor.org/stable/1268522, doi:10.2307/1268522.

Nechak, L., Berger, S., Aubry, E., 2011. A polynomial chaos approach to the robust analysis of the dynamic behaviour of friction systems. European Journal of Mechanics - A/Solids 30, 594 – 607. URL: http://www.sciencedirect.com/science/article/pii/S0997753811000258, doi:https://doi.org/10.1016/j.euromechsol.2011.03.002.

Nechak, L., Berger, S., Aubry, E., 2012. Prediction of random self friction-induced vibrations in uncertain dry friction systems using a multi-element generalized polynomial chaos approach. Journal of Vibration and Acoustics 134, 041015. URL: http://dx.doi.org/10.1115/1.4006413, doi:10.1115/1.4006413.

Nechak, L., Berger, S., Aubry, E., 2013. Non-intrusive generalized polynomial chaos for the robust stability analysis of uncertain nonlinear dynamic friction systems. Journal of Sound and Vibration 332, 1204 – 1215. URL: http://www.sciencedirect.com/science/article/pii/S0022460X12008462, doi:http://dx.doi.org/10.1016/j.jsv.2012.09.046.

Nouy, A., 2009. Recent developments in spectral stochastic methods for the numerical solution of stochastic partial differential equations. Archives of Computational Methods in Engineering 16, 251–285. doi:10.1007/s11831-009-9034-5.

Oden, J., Martins, J., 1985. Models and computational methods for dynamic friction phenomena. Computer Methods in Applied Mechanics and Engineering 52, 527–634. doi:10.1016/0045-7825(85)90009-X.

Renault, A., Massa, F., Lallemand, B., Tison, T., 2016. Experimental investigations for uncertainty quantification in brake squeal analysis. Journal of Sound and Vibration 367, 37 – 55. URL: http://www.sciencedirect.com/science/article/pii/S0022460X16000031, doi:https://doi.org/10.1016/j.jsv.2015.12.049.

Sapsis, T.P., Vakakis, A.F., Bergman, L.A., 2011. Effect of stochasticity on targeted energy transfer from a linear medium to a strongly nonlinear attachment. Probabilistic Engineering Mechanics 26, 119 – 133. URL: http://www.sciencedirect.com/science/article/pii/S0266892010000998, doi:https://doi.org/10.1016/j.probengmech.2010.11.006.

Sarrouy, E., Dessombz, O., Sinou, J.J., 2013. Piecewise polynomial chaos expansion with an application to brake squeal of a linear brake system. Journal of Sound and Vibration 332, 577 – 594. URL: http://www.sciencedirect.com/science/article/pii/S0022460X12006980, doi:https://doi.org/10.1016/j.jsv.2012.09.009.

Schuëller, G., 2001. Computational stochastic mechanics – recent advances. Computers & Structures 79, 2225 – 2234. URL: http://www.sciencedirect.com/science/article/pii/S0045794901000785, doi:https://doi.org/10.1016/S0045-7949(01)00078-5.

Sigalov, G., Gendelman, O.V., AL-Shudeifat, M.A., Manevitch, L.I., Vakakis, A.F., Bergman, L.A., 2012. Resonance captures and targeted energy transfers in an inertially-coupled ro-

tational nonlinear energy sink. Nonlinear Dynamics 69, 1693–1704. URL: https://doi.org/10.1007/s11071-012-0379-1, doi:10.1007/s11071-012-0379-1.

Sinou, J.J., Jézéquel, L., 2007. Mode coupling instability in friction-induced vibrations and its dependency on system parameters including damping. European Journal of Mechanics, A/Solids 26, 106–122. doi:10.1016/j.euromechsol.2006.03.002.

Tison, T., Heussaff, A., Massa, F., Turpin, I., Nunes, R., 2014. Improvement in the predictivity of squeal simulations: Uncertainty and robustness. Journal of Sound and Vibration 333, 3394 – 3412. URL: http://www.sciencedirect.com/science/article/pii/S0022460X14001916, doi:https://doi.org/10.1016/j.jsv.2014.03.011.

Trinh, M., Berger, S., Aubry, E., 2016. Stability analysis of a clutch system with multi-element generalized polynomial chaos. Mechanics & Industry 17, 205. URL: https://doi.org/10.1051/meca/2015061, doi:10.1051/meca/2015061.

Vakakis, A., Gendelman, O., 2001. Energy pumping in nonlinear mechanical oscillators: Part II - Resonance capture. Journal of Applied Mechanics 68, 42–48.

Vakatis, A.F., Gendelman, O.V., Bergman, L.A., McFarland, D.M., Kerschen, G., Lee, Y.S., 2008. Nonlinear Targeted Energy Transfer in Mechanical and Structural Systems. Springer-Verlag, Berlin, New York.

Wan, X., Karniadakis, G.E., 2005. An adaptive multi-element generalized polynomial chaos method for stochastic differential equations. Journal of Computational Physics 209, 617 – 642. URL: http://www.sciencedirect.com/science/article/pii/S0021999105001919, doi:https://doi.org/10.1016/j.jcp.2005.03.023.

Wang, D., Mo, J., Liu, M., Ouyang, H., Zhou, Z., 2016. Noise performance improvements and tribological consequences of a pad-on-disc system through groove-textured disc surface. Tribology International 102, 222 – 236. URL: http://www.sciencedirect.com/science/article/pii/S0301679X16301232, doi:https://doi.org/10.1016/j.triboint.2016.05.030.

Wiener, N., 1938. The homogeneous chaos. American Journal of Mathematics 60, 897. doi:10.2307/2371268.

Xiu, D., Karniadakis, G., 2002. The wiener–askey polynomial chaos for stochastic differential equations. SIAM Journal on Scientific Computing 24, 619–644. URL: http://dx.doi.org/10.1137/S1064827501387826, doi:10.1137/S1064827501387826, arXiv:http://dx.doi.org/10.1137/S1064827501387826.